INTERNATIONAL JOURNAL OF PRECISION ENGINEERING AND MANUFACTURING Vol. 15, No. 11, pp. 2251-2256 NOVEMBER 2014 / 2251
DOI: 10.1007/s12541-014-0588-2

Development of a High Precision Coplanar Stage by using Miniature Michelson Interferometer

Kuang-Chao Fan[1,2], Hao Zhou[1,#], and Ruijun Li[1]

1 School of Instrument Science and Opto-electronic Engineering, Hefei University of Technology, 193,Tunxi Road, Hefei, China
2 Department of Mechanical Engineering, National Taiwan University, Taiwan
Corresponding Author / E-mail: hfutzhouhao@gmail.com, TEL: +86-0551-62903823, FAX: +86-0551-62903823

KEYWORDS: Motion control, Coplanar XY-stage, Back propagation neural network, Abbe error

The motion control of a high precision coplanar XY-stage is very important to the performance of the nano-positioning control system. A prototype micro-coordinate measuring machine (Micro-CMM) has been developed by the authors' group. This system is constructed by a high precision coplanar stage that conforms to Abbe principle, a Z-ram equipped with a touch scan probe and mounted on a pagoda bridge. In this paper, an improved coplanar stage is presented. The miniature laser interferometer based on Michelson principle is developed for precise displacement feedback in each axis and the software for the coplanar stage based on BPNN (Back Propagation Neural Network) in association with the PID control has been developed. Experiment results show that, calibrated by a commercial laser interferometer, the positioning accuracy is proved within 20 nm with a standard deviation less than 15 nm for the travel length of 20 mm.

Manuscript received: January 27, 2014 / Revised: May 29, 2014 / Accepted: July 15, 2014

1. Introduction

Due to rapid advances in the nanotechnology field in recent years, there is an urgent demand for highly-precise measurement system capable of determining the three-dimensional geometries of manufactured components at the micro/nano scale. The author's group has developed two types of micro-CMMs with nanometer accuracy and resolution.[1, 2] The latest one is of a pagoda bridge type, as shown in Fig. 1. This system is constructed by a high precision coplanar stage that conforms to Abbe principle, a Z-ram equipped with a touch scan probe and mounted on a pagoda bridge. The coplanar stage is defined that the X and Y motions are along the common base plane, rather than the conventional stack-up type. In order to meet the requirements of Abbe principle, our coplanar stage was originally constructed by: a moving table on a common base plane, four linear slides (LS1 to LS4) to guide the table, two ultrasonic motors (USM) to actuate the table, two linear displacement grating interferometers (LDGI) to sense X and Y motions[3] and four linear slides (LS5 to LS8) to guide the motions of four arms, as schematically shown in Fig. 2. Having tested, it was found that the grating motion has geometrical angular errors that would cause position counting error of the LDGI.[4] It was determined to redesign the coplanar stage without using LDGIs.

Many long-stroke nano-positioning stages are equipped with commercial laser interferometer as position feedback sensor,[5,6] but laser interferometer is bulky in size and high cost. Considering those shortages, we decided to develop a novel miniature laser interferometer and equip it into a newly designed co-planar stage. The software based motion control system was accordingly developed. Details are described in the following sections.

2. Design of the New Coplanar Stage

2.1 Structure of the coplanar X-Y stage

In general, an X-Y stage can be divided into two main classes, namely the stack-up type and the coplanar type. The former is stacked up by two linear stages that provide displacements in X and Y directions, respectively.[7] Even though the two stages may individually possess a nanoscale positioning accuracy, it is still difficult to achieve good positioning performance due to assembly errors, component misalignment and control error and so on. Moreover, the displacement of the lower stage is subject to large Abbe offset in the vertical direction.

As seen from Fig. 2, the central moving table is pushed and pulled

Fig. 1 Photo of pagoda type micro-CMM

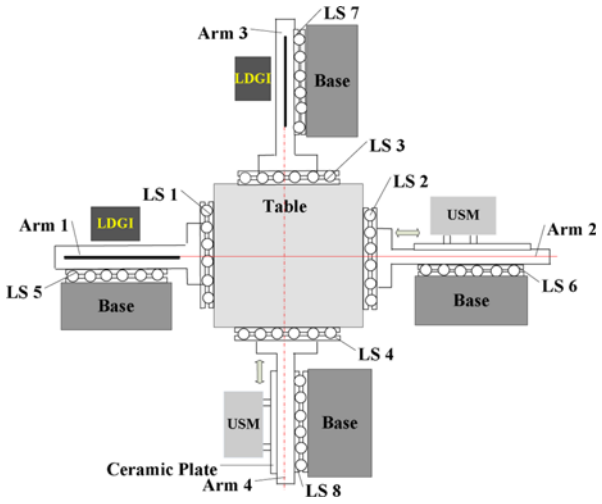

Fig. 2 Schematic diagram of original coplanar stage

by LS6 and LS8 which are actively driven by the ultrasonic motors. In each axis, on the opposite side of the motor, a holographic grating on the linear slide (LS5 or LS7) is passively pushed and pulled by the moving table. LS5 and LS6 are coaxial, which intersects with another coaxial line comprised of LS7 and LS8 perpendicularly. The intersecting point is the probing point of the Micro-CMM. In practice, however, the grating's angular motion in yaw along the slide will introduce additional signal counting of the LDGI, causing positioning error.[4] Moreover, the grating's pitch error is different from the table's pitch error because they are not on the same moving part, incurring another error. In view of these disadvantages, a new coplanar stage has been developed, as schematically shown in Fig. 3. It can be seen that the LDGI has been replaced by the miniature Michelson interferometer. This new coplanar stage eliminates errors caused by LDGI as mentioned above, remains the same symmetrical structure, uses less mechanical components and mostly importantly, adopts a diode laser to reduce the overall size and cost. The function of each part is explained below.

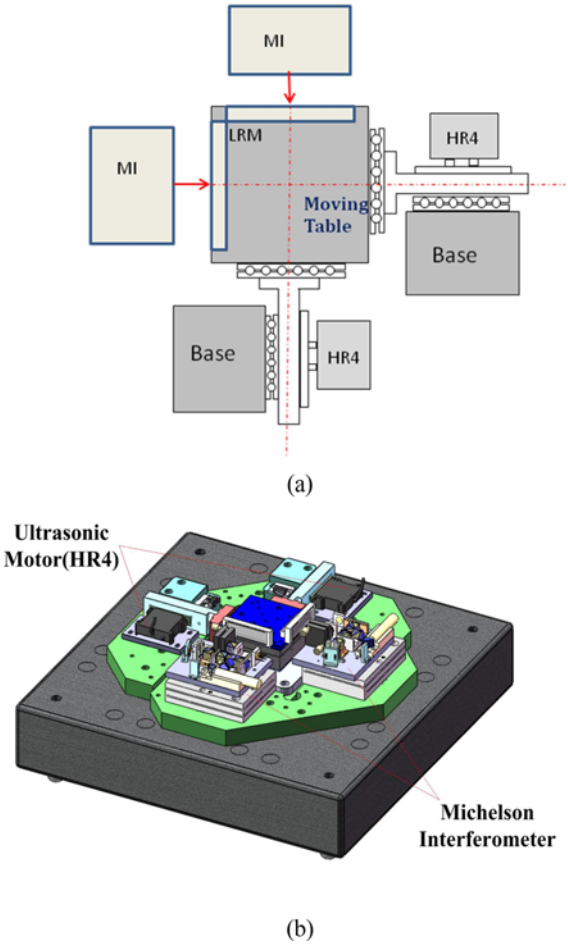

Fig. 3 The developed new coplanar stage, (a)Schematic diagram, (b) CAD structure design

2.2 The driving system

As shown in Figs. 2 and 3, the linear slide of each axis is driven by an actuator system comprising an ultrasonic motor (HR4) and a corresponding driver amplifier (model AB2), made by Nanomotion Co. of Israel. Our previous study has confirmed the effectiveness of this single actuator for long-stroke and nanopositioning on a commercial linear stage.[8, 9] A brief description is as follows.

The HR4 has four piezoelectric elements. The AB2 drive box received control signal from the NI PCI-6259, which is connected to the computer, and converts the input command signal into a corresponding PWM output signal. The output transformer-amplifier circuit converts the PWM output signal into a high voltage sine wave that drives the motor HR4.Then the front edge of the motor generates an elliptical motion, which is the vector sum of the bending mode and the longitudinal mode, as shown in Fig. 4. In this study, we use three motion modes to accommodate different scales, namely AC, Gate and DC modes. As shown in Fig. 5, in AC mode, motor HR4 generates a successive motion at the speed of 0.5 mm/s with a Neural Network PID Controller to the position about 2 μm before the target. Then, in GATE mode, motor HR4 drives the XY-stage in pulses with short steps of 20~50 nm and the average speed is controlled to 25 μm/s to the position about 50 nm before the target. Finally in DC mode, HR4 works like a conventional PZT actuator with lower speed and nanometer steps to the

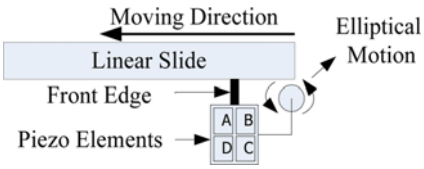

Fig. 4 Actuation principle of HR 4

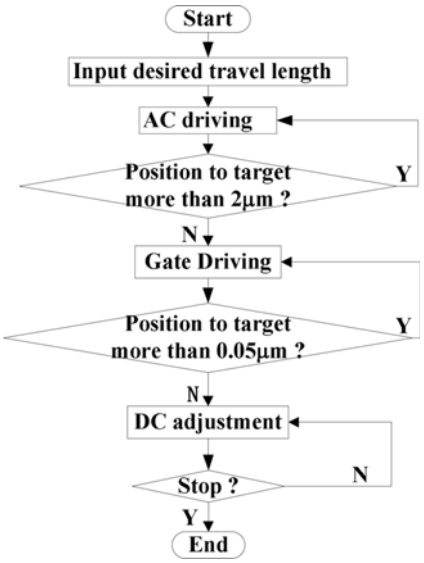

Fig. 5 Integration of 3 driving modes to achieve nanopositioning accuracy

target position. Through the integration of 3 driving modes, long stroke and nanopositioning accuracy can be achieved.[9,10]

2.3 Miniature michelson interferometer

In order to be equipped into the Micro-CMM, the coplanar stage has limited space for the displacement sensors to nanometer resolution and accuracy. Considering that commercial laser interferometer is too bulky, a miniature laser interferometer for precise displacement feedback in each axis has been developed, as illustrated in Fig. 6. A partially polarized laser beam of 635 nm wavelength from the laser diode (LD) impinges on the polarizing beam splitter PBS1 and is split into two beams: the transmitted P-beam and the reflected S-beam. The reflected beam is reflected by the fixed reference mirror, and the transmitting is reflected by the moving mirror mounted on the stage. The displacement of the moving mirror will cause the optical path difference between the two reflected beams so as to produce interference. The quarter wave-plates Q1 and Q2 prevent the reflected beams from going back into the laser diode, because each polarization state will be changed by 90º after passing a quarter waveplate twice. The two reflected beams are combined at PBS1 and converted into left and right circularly polarized beams by Q3. With the phase shift module composed by NPBS, PBS2 and PBS3, the interference fringe with 90º phase shift can be detected by photo-detectors PD1 to PD4. Analyzed by Jones vector, the intensity of each photo-detector can be expressed as:

$$I_{PD1} = A\left[1-\cos\left(\frac{2\pi d}{\lambda}\right)\right] \quad (1)$$

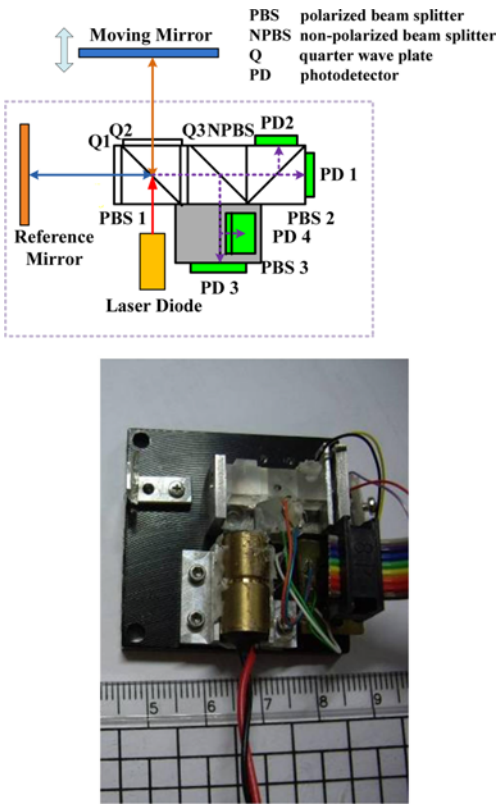

Fig. 6 Schematic diagram and photo of miniature Michelson interferometer

$$I_{PD2} = A\left[1+\cos\left(\frac{2\pi d}{\lambda}\right)\right] \quad (2)$$

$$I_{PD3} = A\left[1+\sin\left(\frac{2\pi d}{\lambda}\right)\right] \quad (3)$$

$$I_{PD4} = A\left[1-\sin\left(\frac{2\pi d}{\lambda}\right)\right] \quad (4)$$

Where, A and λ are the intensity and the wavelength of the laser beam, and d is the optical path difference of the two reflected beams. Processing the current signal with the operation of (PD3–PD4) and (PD2–PD1), two orthogonal sinusoidal signals with $\pi/2$ phase shift can be obtained.

$$S_1 = 2A\left(\sin\frac{2\pi d}{\lambda}\right) \quad (5)$$

$$S_2 = 2A\left(\cos\frac{2\pi d}{\lambda}\right) \quad (6)$$

The displacement of the moving mirror (X) will generate one half of the optical path difference, so that $2X=d$. Therefore, the phase changes of the two sinusoidal signals can be expressed by the following equation.

$$\theta = \tan^{-1}\left(\frac{S_1}{S_2}\right) = \frac{4\pi X}{\lambda} \quad (7)$$

During the motion of the moving mirror, the interference fringe will be kept changing with the period of one-half wavelength ($\lambda/2$). The total displacement of the moving mirror can be expressed by the following equation.

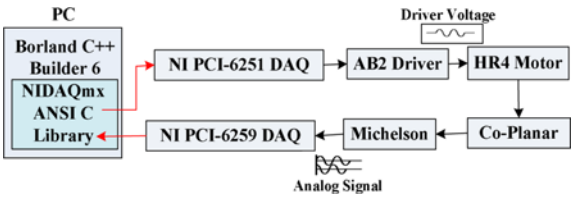

Fig. 7 Block diagram of control loop for coplanar X-Y stage

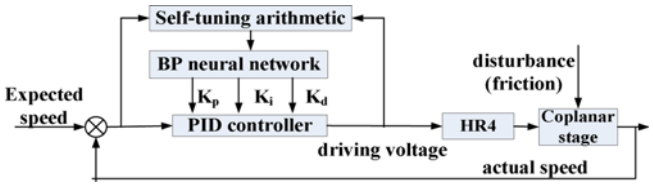

Fig. 8 Block diagram of self-tuning PID controller

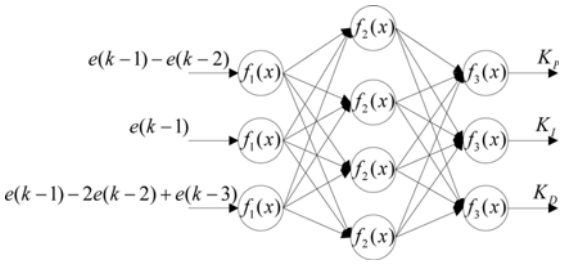

Fig. 9 BPNN network

$$X=\frac{\lambda}{2}(N+\tan\theta_i+\tan\theta_f) \tag{8}$$

Where, θ_i and θ_f are the phases of initial and final incomplete wave cycles, respectively. With the developed software in PC carrying out pulse counting (for N) and phase subdivision (for θ_i and θ_f), the displacement can be calculated to nanometer resolution if the phase can be detected to one degree, which is a pretty normal technique. A software based signal subdivision technique has been developed by the author's group.[11] The physical dimension of the developed miniature Michelson interferometer is about (4.5×4.5×3) cm^3, as shown in Fig. 6.

2.4 Self-tuning PID control algorithm

When choosing a suitable driving system, the ultrasonic motor has the advantages of compact structure and the capability of integrating multi-scale driving modes in an all-in-one actuator. Its motion scheme, however, still remains a challenging task because the friction change along the common base plane affects the stability obviously, especially for low-speed and long-stroke control. Conventional PID controller with fixed parameters cannot overcome the problem when the uneven surface friction generates large velocity variation. So we have developed a software-based controller around the Borland C++ Builder environment in a PC. The block diagram of control loop for coplanar X-Y stage is shown in Fig. 7. The motion control system comprises actuation system (two USM and associated driver amplifiers), displacement sensors and

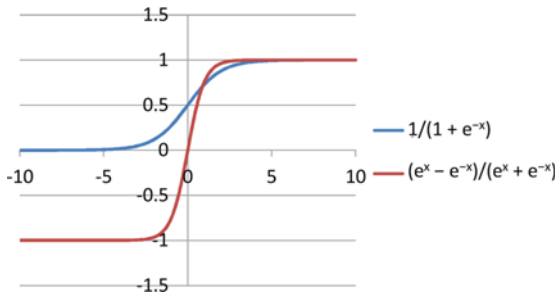

Fig. 10 Convergent rates of two different transfer functions

a self-tuning PID controller. The PC gets displacement signals via a NI (National Instrument Co.) DAQ (Data Acquisition) card. As shown in Fig. 8, the PID parameters are adjusted in real-time by a BPNN[12] in accordance with the difference between the desired value and the actual value. In constructing the BPNN, the network has three layers, namely input layer, hidden layer and output layer, as shown in Fig. 9. The nodes in the input layer receive three sets of errors, namely [e(k-1)-e(k-2)], e(k-1) and [e(k-1)-2e(k-2)+e(k-3)], as inputs, while those in the output layer provide the proportional, integral and derivative gains as outputs. The total input and output to each neuron j(net$_j$) in hidden and output layers are defined as follows:

$$\begin{cases} net_j^n=\sum_{j=1}^{M}\omega_{ij}y_j^{n-1}-\theta_j \\ y_j^n=f_i[net_j^n] \end{cases} \tag{9}$$

where θ is the pre-defined threshold value, ω is weight coefficient, y is the output of each neuron and $f(x)$ is the transfer function. When choosing the transfer function, convergence rate is a major factor. Experiments show that compared with the sigmoid function tanh(x) converges faster, as shown in Fig. 10. As to each layer, $f(x)$ is defined as follows:

$$\begin{cases} f_1(x)=x \\ f_2(x)=(e^x-e^{-x})/(e^x-e^{-x}) \\ f_3(x)=0.5\times(1.0+(e^x-e^{-x})/(e^x-e^{-x})) \end{cases} \tag{10}$$

In implementing the BPNN, the cost (error) function is defined as

$$e(k)=\frac{1}{2}\times\Sigma(r(k)-y(k))^2 \tag{11}$$

Eq. (11) expresses the difference between the desired output $r(k)$ and the actual output $y(k)$. The objective of the BPNN is to determine the PID gains which minimize the cost function using gradient descent method. The BPNN-based incremental PID controller is then formulated as

$$u(k)=K_Pe(k)+K_I[e(k)-2e(k-1)+e(k-2)]+K_D[e(k)-e(k-1)] \tag{12}$$

Where K_P, K_I and K_D are the proportional, integral and derivative gains; $u(k)$ is the drive voltage increment and $e(k)$ is the control error.

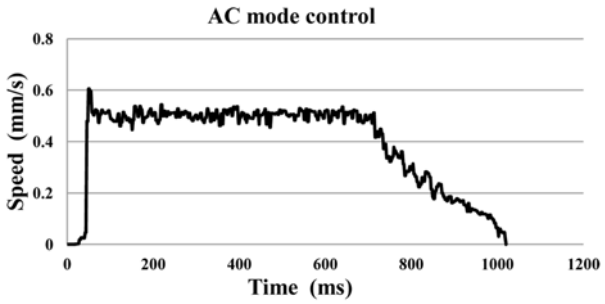

Fig. 11 AC-mode control self-tuning PID controller

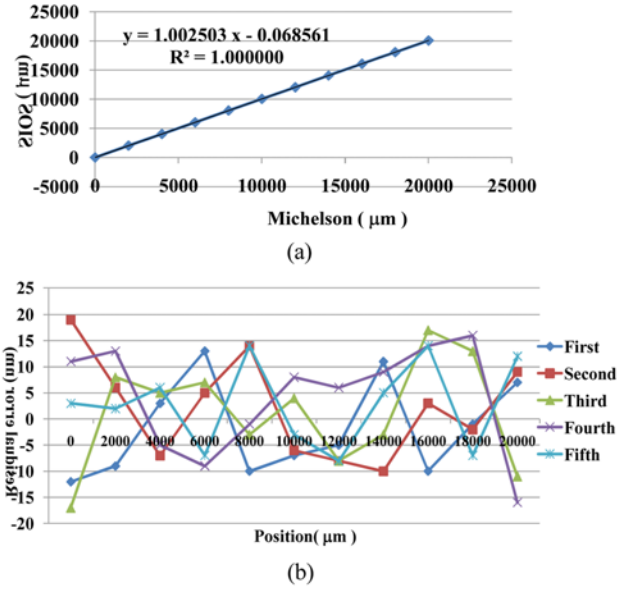

Fig. 12 Positioning error calibration, (a) before cosine error compensation, (b) after cosine error compensation

3. Experiments

3.1 BPNN used in AC mode to control speed

In AC mode the stage's speed is controlled to 0.5 mm/s for 0.1~20 mm motion; in Gate mode the step size is controlled for motion in micrometer range; and in DC mode the displacement is controlled in nanometer range. As mentioned above, the friction change along the guide way affects the stability, Fig. 11 shows the speed control performance obtained in the AC mode using the BPNN-based PID controller. It is evident that the BPNN-based controller successfully eliminates the overshoot phenomenon in the initial displacement period, suppresses the variation in the slide velocity over the middle travel and decreases the speed progressively in the last stage.

3.2 Positioning experiment

A SIOS SP-2000 laser interferometer was used to calibrate the positioning accuracy of the XY-stage. The positioning errors were obtained by comparing the reading of Michelson interferometer with that of SIOS at every 2 mm from 0 mm to 20 mm. Each experiment was repeated by 5 times at the same position. As the optical axis of SIOS may not be perfectly aligned with the motion axis of the stage, with a little alignment angle it leads to a significant cosine error. So the experimental data of the first test were fitted by a least-squares line to obtain a compensation function, as shown in Fig. 12(a) for the X motion. Then in the second test, the readings of Michelson interferometer were corrected by the compensation function (X'=1.002503X-0.068561), where X is the commanded position and X' is the compensated position. The positioning errors were controlled to within 20 nm with a standard deviation less than 15 nm, as shown in Fig. 12(b).

4. Conclusions

In this paper, an improved symmetrical coplanar XY-stage is proposed. Each axis is driven by the ultrasonic motor HR4 and detected by the Michelson interferometer. A BPNN control scheme has been developed by software. Positioning experiment results show that this coplanar stage has achieved less than 20 nm positioning accuracy and within 15 nm standard deviation for travels up to 20 mm after compensation of systematic errors. It is integrated into a micro-CMM and used for the XY motion.

REFERENCES

1. Fan, K. C., Fei, Y. T., Yu, X. F., Chen, Y. J., Wang, W. L., et al., "Development of a Low-Cost Micro-CMM for 3D Micro/Nano Measurements," Measurement Science and Technology, Vol. 17, No. 3, pp. 524-532, 2006.
2. Fan, K. C., Cheng, F., Wang, H. Y., and Ye, J. K., "The System and the Mechatronics of a Pagoda Type Micro-CMM," International Journal of Nanomanufacturing, Vol. 8, No. 1, pp. 67-86, 2012.
3. Cheng, F. and Fan, K. C., "Linear Diffraction Grating Interferometer with High Alignment Tolerance and High Accuracy," Applied Optics, Vol. 50, No. 22, pp. 4550-4556, 2011.
4. Fan, K. C., Zhang, Y. L., Miao, J. W., and Cheng, F., "Error Compensation of Grating Interferometer due to Angular Error of Linear Stage," Proc. of IEEE/ASME International Conference on Advanced Intelligent Mechatronics (AIM), pp. 428-431, 2012.
5. Kramar, J. A., "Nanometre Resolution Metrology with the Molecular Measuring Machine," Measurement Science and Technology, Vol. 16, No. 11, pp. 2121-2128, 2005.
6. Liu, C. H., Jywe, W. Y., Jeng, Y. R., Hsu, T. H., and Li, Y. T., "Design and Control of a Long-Traveling Nano-Positioning Stage," Precision Engineering, Vol. 34, No. 3, pp. 497-506, 2010.
7. Polit, S. and Dong, J., "Development of a High-Bandwidth XY Nanopositioning Stage for High-Rate Micro-/Nanomanufacturing," IEEE/ASME Transactions on Mechatronics, Vol. 16, No. 4, pp. 724-733, 2011.
8. Fan, K. C., Cheng, F., and Chen, Y. J., "Nanopositioning Control on a Commercial Linear Stage by Software Error Correction,"

Nanotechnology and Precision Engineering, Vol. 4, No. 1, pp. 1-9, 2006.

9. Fan, K. C. and Lai, Z. F., "An Intelligent Nano-Positioning Control System Driven by an Ultrasonic Motor," Int. J. Precis. Eng. Manuf., Vol. 9, No. 3, pp. 40-45, 2008.
10. Cheng, F., Fan, K. C., Miao, J., Li, B. K., and Wang, H. Y., "A BPNN-PID based Long-Stroke Nanopositioning Control Scheme Driven by Ultrasonic Motor," Precision Engineering, Vol. 36, No. 3, pp. 485-493, 2012.
11. Fan, K. C. and Cheng, F., "LDGI Signal Subdivision by Soft Computing for Nanomeasurement," Proc. of 6th International Symposium on Precision Engineering Measurements and Instrumentation, Vol. 7544, 2010.
12. Omatu, S. and Yoshioka, M., "Self-Tuning Neuro-Pid Control and Applications," Proc. of IEEE International Conference on Systems, Man, and Cybernetics, pp. 1985-1989, 1997.